

Journal Pre-proof

Influence of TiO₂ on the densification behaviour of Yb₂O₃

Sanat Chandra Maiti, Quan Li, Fei Peng, Rajendra Bordia



PII: S0955-2219(21)00589-6

DOI: <https://doi.org/10.1016/j.jeurceramsoc.2021.08.022>

Reference: JECS 14265

To appear in: *Journal of the European Ceramic Society*

Received Date: 16 March 2021

Revised Date: 27 June 2021

Accepted Date: 13 August 2021

Please cite this article as: { doi: <https://doi.org/>

This is a PDF file of an article that has undergone enhancements after acceptance, such as the addition of a cover page and metadata, and formatting for readability, but it is not yet the definitive version of record. This version will undergo additional copyediting, typesetting and review before it is published in its final form, but we are providing this version to give early visibility of the article. Please note that, during the production process, errors may be discovered which could affect the content, and all legal disclaimers that apply to the journal pertain.

© 2020 Published by Elsevier.

Influence of TiO₂ on the densification behaviour of Yb₂O₃

Sanat Chandra Maiti, Quan Li⁺, Fei Peng, Rajendra Bordia *

Department of Materials Science and Engineering, Clemson University, Clemson, South Carolina, USA

⁺ Current Affiliation: College of Materials Science and Engineering, Nanjing Tech University, Nanjing, Jiangsu Province, 211816, China

*Corresponding author (rbordia@clemson.edu)

Abstract:

The effect of temperature and heating rate on the densification of ytterbia (Yb₂O₃), with and without titania (TiO₂) doping was investigated. It is shown that up to a certain doping level, titania doping enhances the densification behaviour of ytterbia. The effect of titania doping on crystal structure confirms that titania is substitutionally incorporated in ytterbia up to the solubility limit, which corresponds well with the densification results. The increased densification rate of titania-doped ytterbia is attributed to the formation of cation vacancy and lattice distortion. Using constant heating rate experiments, the activation energy for densification has been calculated and it is shown that in the intermediate density range (60 % to 85 %), the activation energy is independent of the density. Titania doping increases the activation energy for densification.

1. Introduction:

Ytterbia, Yb₂O₃, is of significant interest as a transparent ceramics for high-power laser applications due to its higher thermal conductivity than YAG [1–3], and Yb₂O₃ films have been used as sensing films in the pH-ion sensitive field-effect-transistor devices, memory cells, and high-k gate insulators [4–6]. In addition, ytterbia is an excellent sintering aid for a variety of ceramics, including Si₃N₄ [7–9], MgO [10], AlN [11], SiC-AlN [12], and ZrB₂ [13]

leading to improvement in their mechanical properties. Finally, ytterbia based infra-red reflective coatings have been investigated to protect the equipment against the external heating in aero-space applications [14]. Although there are all these current and potential applications, fundamental investigations on the sintering behaviour of ytterbia, similar to the kind of detailed investigations that have been conducted for other oxides, like Y_2O_3 , ZrO_2 , Al_2O_3 , CeO_2 are lacking. The sintering behaviour of these other oxides has been well investigated using different approaches [15–22]. For many of these oxides, suitable dopants have also been identified to enhance the densification at a lower temperature [18,23–28]. For example, Rahaman and Zhou [29] investigated the role of different additives (Mg^{2+} , Ca^{2+} , Sc^{3+} , Y^{3+} and Nd^{3+}) on the sintering of ultra-fine CeO_2 powders. They have shown that the dopants had a dramatic effect on sintering and grain growth behaviour. Lee et al. [30] has shown the influence of gadolinium oxide on the sintering behaviour of ceria. They reported that increased sintered density in the presence of gadolinium oxide is due to the generation of cation vacancy. Similarly, the influence of doping on sintering kinetics for ZrO_2 and Al_2O_3 is well documented [23,28,31–36]. Jung et al. recently showed that titania doping improves the densification of sub-micrometer Y_2O_3 powder by increasing the grain boundary mobility. They have also shown that two-step sintering process is more efficient than a single step for titania doped Y_2O_3 [18]. The focus of this investigation is the sintering kinetics of Yb_2O_3 . As TiO_2 has been shown to be an effective dopant to reduce the sintering temperature and enhance densification for Y_2O_3 and ZrO_2 ceramics. In this paper, we report the effect of TiO_2 doping on the densification behaviour and sintering kinetics at different temperatures of Yb_2O_3 ceramics.

2. Experimental procedure:

(a) Powder preparation and characterization techniques:

Yb_2O_3 powders (3-5 μm , purity: 99.9%) were used in this study (Sky Spring Nanomaterials, Houston, USA). TiO_2 particles with an average particle size 300 nm were used (Nanophase Technologies Corporation, Illinois, USA). First, the particle size of the Yb_2O_3 powders was reduced to the submicron particle by milling the powders using zirconia milling media (Inframat Advanced Materials, Manchester, USA) with isopropanol on a ball mill for five days (weight ratio of powder: zirconia milling media of 1:4). After milling, isopropanol was evaporated at 80°C and 300 mbar for 2 hrs. The distribution of particle size was measured using a particle size analyser (Shimadzu, SALD-2300, Japan), and the measured median value was ~ 510 nm. To see the influence of additive, different mole percentages (3, 5 and 10 mole%), of TiO_2 was mixed with the milled Yb_2O_3 powders in isopropanol on a roller mixer for 1 day using zirconia milling media. The powders were dried using the same procedure as for pure Yb_2O_3 powders. The final step was drying of the powders at 120°C for 12 hrs in the air to remove any organic residue. After drying, the powders were uniaxially pressed into pellets at a pressure of 10 MPa. Finally, these pellets were sintered in air (CM Furnaces, Bloomfield, USA) at different temperatures (1300, 1350 and 1400°C) for 2 hrs. The sintered density and open porosity were determined by the Archimedes method. The skeleton density of the corresponding sample was measured by the Helium pycnometer (Micromeritics AccuPyc 1330, USA). The crystalline phase characterization was carried out using X-ray diffraction (Rigaku Ultima IV diffractometer, Japan) with $\text{Cu K}\alpha$, operating at 40 kV and 40 mA over the angular range of 10-80°. The scan speed was kept at 0.2 s/step with step size 0.005. The lattice parameter was estimated by Rietveld refinement of the XRD data with the help of Fullprof program [37]. The microstructures of the sintered samples were observed by field emission scanning electron microscope (FESEM) (Hitachi 4800, Japan). The cross-section of the samples was polished and thermally etched before the analysis. Thermally etching was done at a temperature 50 °C below the sintering temperature for 15 minutes.

(b) Sintering kinetics:

Uniaxially pressed green compacts of 6 mm diameter and ~ 4mm thickness were prepared for dilatometry experiments. Dilatometry experiments were carried out in a horizontal push rod type dilatometer (Netzsch 402C, Germany). The compacts were heated at four different heating rates (5, 10, 15, and 20 °C/min) up to 1500 °C followed by furnace cooling to room temperature. Only the data during the constant heating rate was analyzed. Using the length change and assuming isotropic shrinkage, the density change was calculated as a function of time [38]. The experimental data obtained by dilatometry were analyzed by Wang and Raj method [23]. In this method, the densification rate can be separated into temperature, density, and grain size-dependent factors. The densification rate can be expressed as follows:

$$\frac{d\rho}{dt} = A \frac{e^{-\frac{Q}{RT}} f(\rho)}{T d^n} \quad (1)$$

Here $\frac{d\rho}{dt}$ is the instantaneous densification rate, A is the pre-exponential factor, R is the universal gas constant, $f(\rho)$ is a function of only density, Q is the activation energy, T is the absolute temperature, d is the grain size, and n is the grain size exponent ($n=3$, when densification rate is controlled by lattice diffusion and $n=4$, it is grain boundary diffusion-controlled). The logarithm of Eq. 1 gives

$$\ln \left(T \beta \frac{d\rho}{dT} \right) = -\frac{Q}{RT} + \ln[f(\rho)] + \ln A - n \ln d \quad (2)$$

Where β is the heating rate (dT/dt). A plot of the left-hand side of Eq. 2 vs. $1/T$ gives a value of Q provided that the data points are taken at a constant value of ρ and d . Assuming that for samples with the same particle size and starting grain density, the grain size, d , is only a function of density [22], considering Eq. (2) at a constant value of ρ for different constant heating rates, values of Q at different values of ρ can be obtained.

Assuming isotropic shrinkage of the powder compact and using the true strain for densification shrinkage (since it is large shrinkage), the time-dependent density was calculated from the following equation [38]:

$$\rho = \left(\frac{L_f}{L(t)}\right)^3 \rho_f \quad (3)$$

Where L_f is the final length measured by calipers, $L(t)$ is the time-dependent length (calculated from dilatometric shrinkage) and ρ_f is the final density of the sample measured by the Archimedes method.

3. Results and discussion:

3.1 Density, porosity and microstructure

The density and open porosity of the samples of Yb_2O_3 sintered at different temperatures as a function of different mole % of titanium doping is shown in Fig. 1(a) and (b), respectively. From these figures, it can be seen that titanium doped Yb_2O_3 ceramics show higher density than the undoped sample, which increases with the percentage of doping and sintering temperatures. The influence of titanium doping on relative density at 1300 °C is less effective than 1350 and 1400°C. The relative density at 1350 °C dramatically increases with increasing titanium doping from 3 to 5 mole % and remains the same at 10 mole% of doping. In contrast, at 1400 °C the relative density increases sharply for 3 mole % doping and remains the same with increasing level of doping. The results indicate that the minimum level of doping for maximum effectiveness for 1350 °C and 1450 °C is 5 and 3 mole %, respectively.

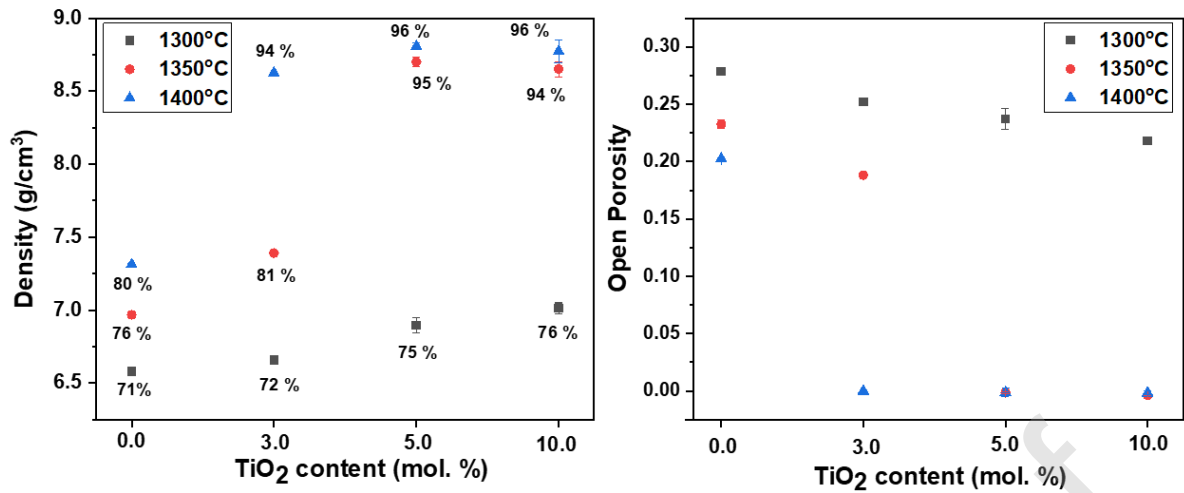


Figure 1: Density and open porosity of doped and undoped samples at different temperatures for 1 h soaking time; relative density of the corresponding samples are mentioned on the graph.

The open porosity of the corresponding samples is shown in Fig. 1 (b). The results indicate that at optimum doping, open porosity drops to zero for samples sintered at 1350 and 1400 °C.

Fig. 2 shows the microstructure of the samples sintered at 1350 °C with different mole% of TiO₂ doping. For undoped Yb₂O₃ (Fig. 2a), a significant amount of porosity is observed, which decreases as doping increases to 3 and 5 mole % (Fig. b and c). No noticeable change in microstructure can be observed for 10 mole% of TiO₂ doping as compared to 5 mole% doping. From these results, it can be concluded that beyond 5 mole% TiO₂ doping does not change the microstructure, which is also supported by relative density (Fig. 1a).

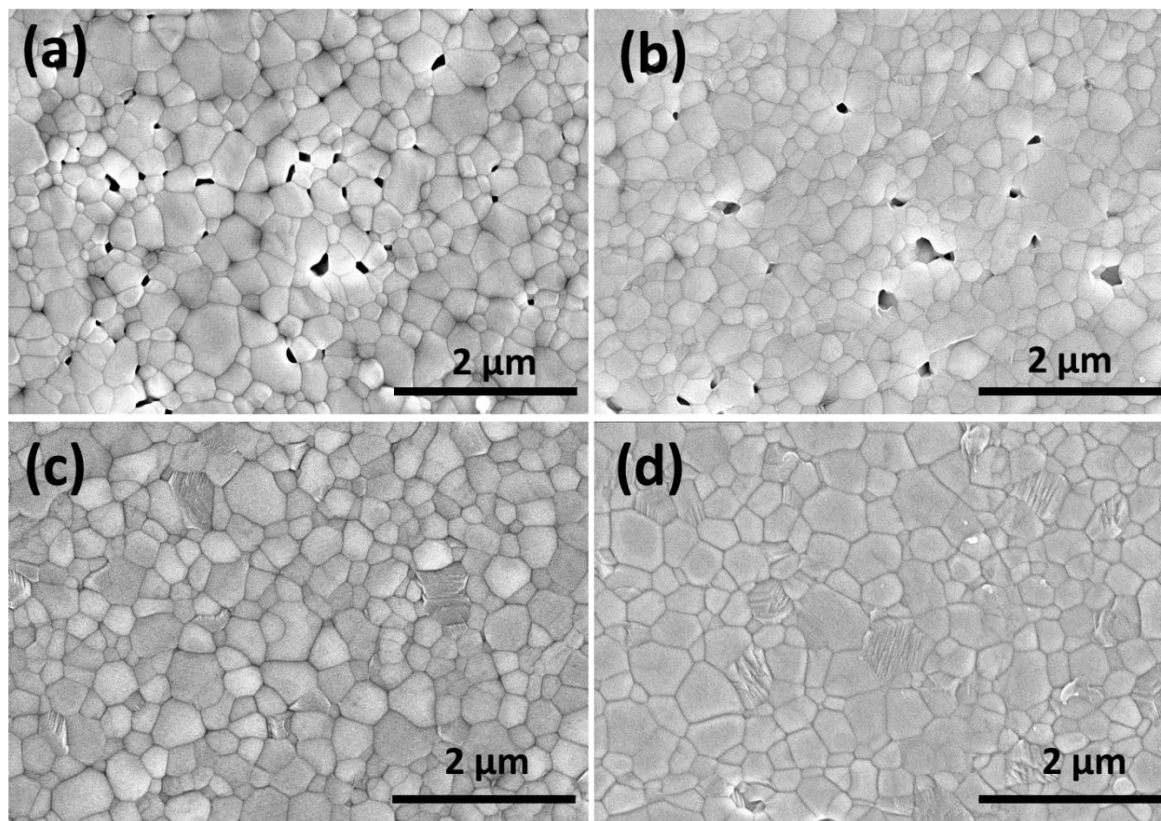
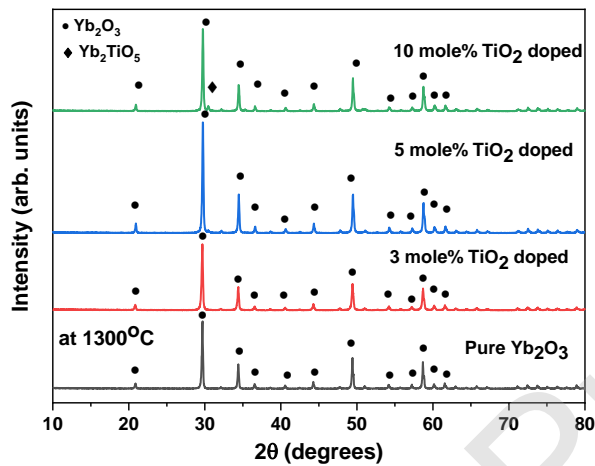


Figure 2. FESEM images of doped and undoped Yb_2O_3 at 1350 °C; (a) pure Yb_2O_3 , (b) 3 mole% doped Yb_2O_3 , (c) 5 mole% doped Yb_2O_3 (d) 10 mole % doped Yb_2O_3

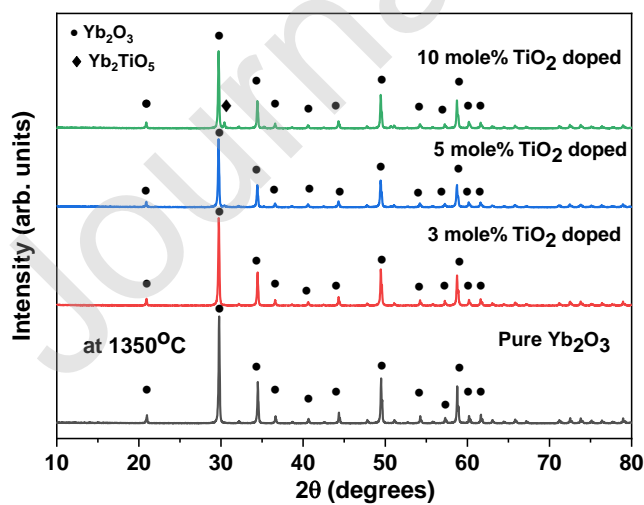
3.2 Crystal structure

In order to study whether Ti ions are incorporated in ytterbia, detailed powder X-ray diffraction (XRD) analysis was conducted. The XRD patterns of doped and undoped samples sintered at different temperatures are shown in Fig. 3 (3 (a) for 1300 °C; 3 (b) for 1350 °C; 3 (c) for 1400 °C). Diffraction peaks in all the compounds are intense and sharp, indicating good crystalline nature of samples with a cubic structure. All the doped samples show similar XRD patterns as that of pure Yb_2O_3 , and no extra diffraction peaks due to TiO_2 are observed (up to 5 mole % doping). The results suggest that the Ti ions have been effectively incorporated into the Yb_2O_3 lattice. At a higher percentage of doping (10 mole% TiO_2) some Yb_2TiO_5 is formed at all these temperatures. Rietveld analysis of the XRD data of pure

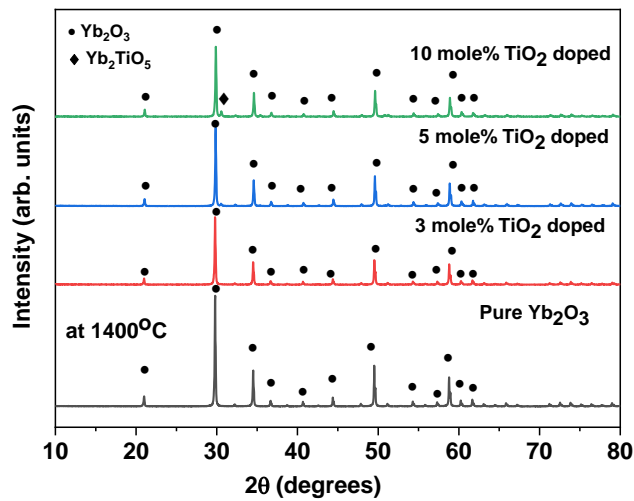
Yb₂O₃ at 1350 °C is shown in Fig. 4. The refined lattice parameter of pure Yb₂O₃ is estimated (10.4379 Å). The low χ^2 (1.722) value of the refinement indicates the good refinement of the XRD data. The change in the lattice parameter for doped samples is estimated by the Rietveld refinement as well and plotted in Fig. 5. It is observed that with increasing the doping level up to 5 mole %, the lattice parameter decreases and then becomes almost constant. Therefore, it is estimated that solid solubility of titania in Yb₂O₃, at 1350 °C should be around 5 mole%. The densification results also are in agreement with this conclusion.



(a)



(b)



(c)

Figure 3. XRD patterns of doped and undoped Yb₂O₃ at different temperatures. (a) at 1300°C, (b) at 1350°C and (c) at 1400°C.

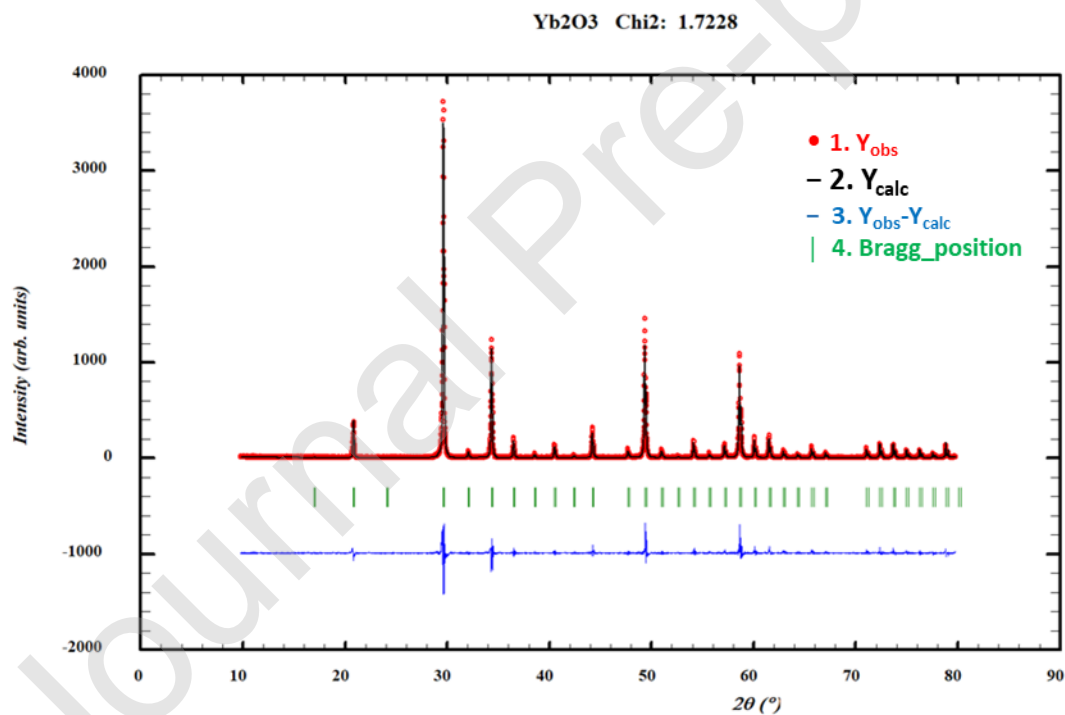


Figure 4. Rietveld analysis of pure Yb₂O₃ after processing in air at 1350°C for 2 h

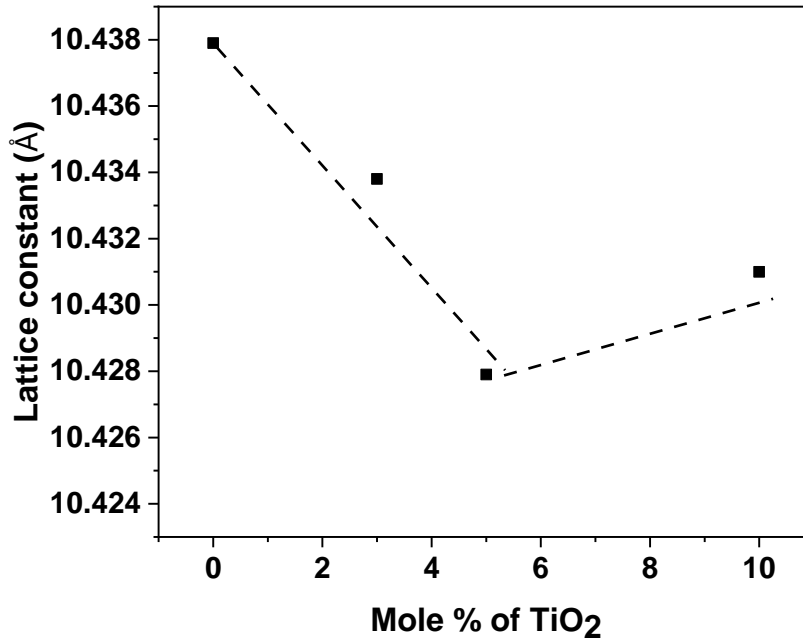
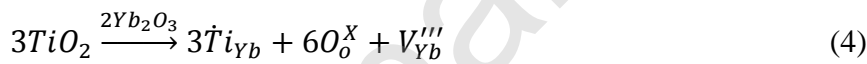


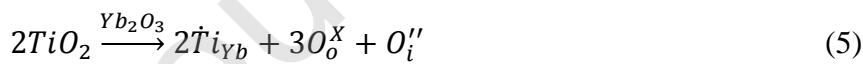
Figure 5. Lattice parameter as a function of TiO₂ content at 1350 °C

It is postulated that TiO₂ additions resulted in the substitution of Ti⁺⁴ ions for Yb⁺³ ions up to the solubility limit. Two possible substitution reactions can be described by using the Kröger-Vink notation as follows:

Charge compensation by Yb⁺³ ion vacancies



Charge compensation by O²⁻ ion in interstitial sites



It is expected that reaction (5) is unlikely as it is quite difficult to form oxygen interstitial due to the large size of the oxygen ions [39]. Therefore, cation vacancy (V_{Yb}''') is the predominant defect due to titania doping (Eq. 4). It is expected that these cation vacancies enhance the diffusion rate of cations and promote grain boundary mobility [19]. Moreover, the addition of TiO₂ could induce significant distortion of the surrounding lattice as the Ti⁺⁴ (0.605 Å) ion

has a much smaller size compared with that Yb^{+3} (0.86 Å) [40]. As a result, it also promotes grain boundary mobility due to lattice distortion [30,41].

As shown in Figure 5, the lattice parameter has a minimum around 5 Mole % TiO_2 doping. The increase in the lattice parameter at higher doping level needs to be investigated further. Since there is only one data point, first, it should be confirmed that this increase is real.

Assuming it is, a possible explanation is that up to 5 Mole %, Ti^{+4} ions substitute for Yb^{+3} ions and beyond 5 Mole %, they go into the interstitial sites until the second phase starts to form. It should be noted that for 10 Mole % TiO_2 doping, the Yb_2TiO_5 impurity phase is observed. It needs to be determined at what doping levels the second phase forms and what is the lattice parameter for this value of doping levels.

Both sintered density and grain size increased with increasing TiO_2 content up to 5 mol% and remains constant for 10 mol% TiO_2 . These results indicate that the addition of TiO_2 enhances the densification within the solubility limit and promote the grain boundary mobility.

Therefore higher density is observed for the TiO_2 doped sample (shown in Fig. 1 and 2).

However, at higher TiO_2 content beyond the solubility range (10 mol %), Yb_2TiO_5 forms (Fig. 3), which resists further grain growth (grain boundary pinning).

3.3 Densification kinetics

Fig. 6 shows the linear shrinkage, at different constant heating rates, for doped as well as undoped samples. Fig. 6 (a) is for pure Yb_2O_3 and Fig. 6 (b), (c), and (d) are shrinkage data for 3, 5, and 10 mole% doped samples. From the figures, it can be seen that no noticeable shrinkage is observed till 1100 °C for all the heating rates, and shrinkage increases with further increase in temperature. For all samples at a particular temperature, shrinkage is highest at 5 K/min and decreases with increasing heating rates.

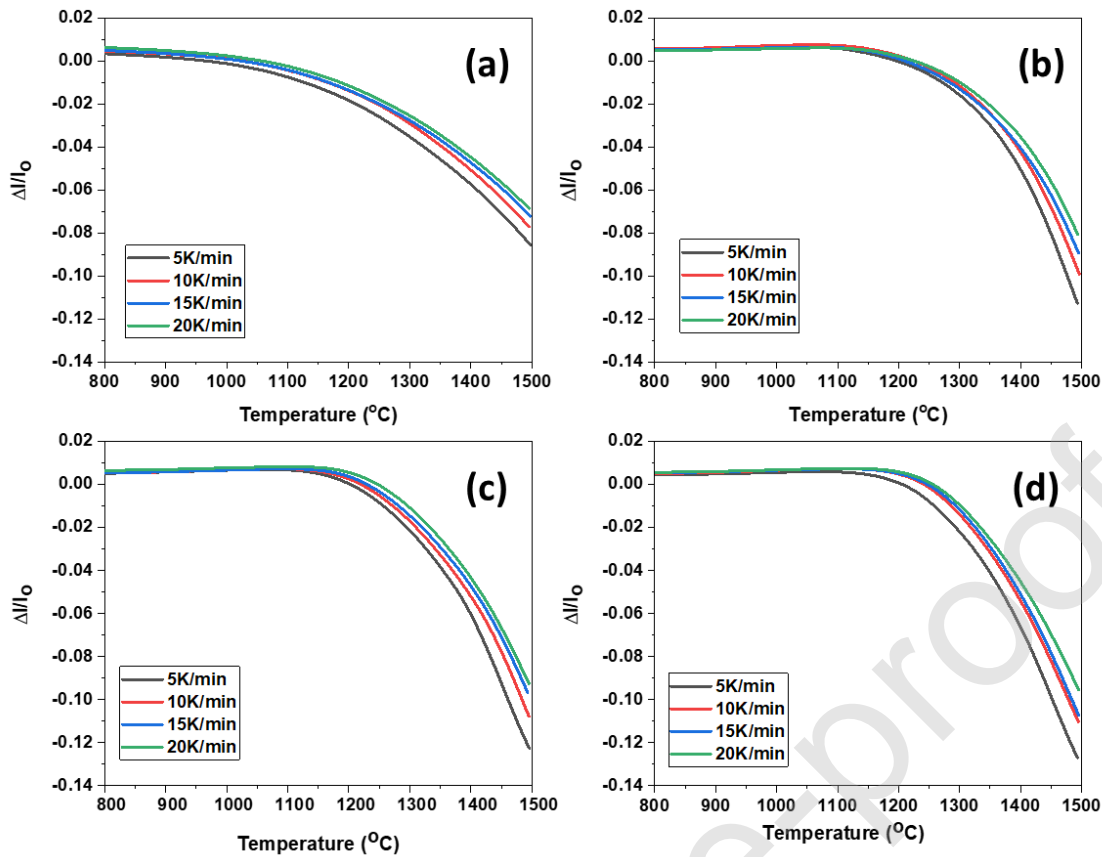


Figure 6. Linear shrinkage as a function of temperature at different constant heating rates; (a) Pure Yb_2O_3 (b) 3 mole% TiO_2 doped Yb_2O_3 (c) 5 mole% TiO_2 doped Yb_2O_3 (d) 10 mole% TiO_2 doped Yb_2O_3 .

The variation of instantaneous relative densities of the samples as a function of temperature calculated using Eq. 3 is shown Fig. 7. Fig. 7 (a) for pure Yb_2O_3 and Fig. 7 (b), (c), and (d) for 3, 5, and 10 mole% doped samples. No change in relative density is observed in all samples up to 1100°C for all heating rates. Beyond 1100 °C, the relative density increases with increasing temperature. At a particular temperature, relative density decreases with increasing heating rates, which is similar to shrinkage variation with the heating rate (Fig. 6). The relative density of pure Yb_2O_3 reaches ~ 80 % at temperature 1500°C with 5K/min heating rate whereas, for doped samples, the value of relative density is close to ~90%. The results suggest that the densification rate increases with the doping of TiO_2 . Similar trends are observed for other heating rates.

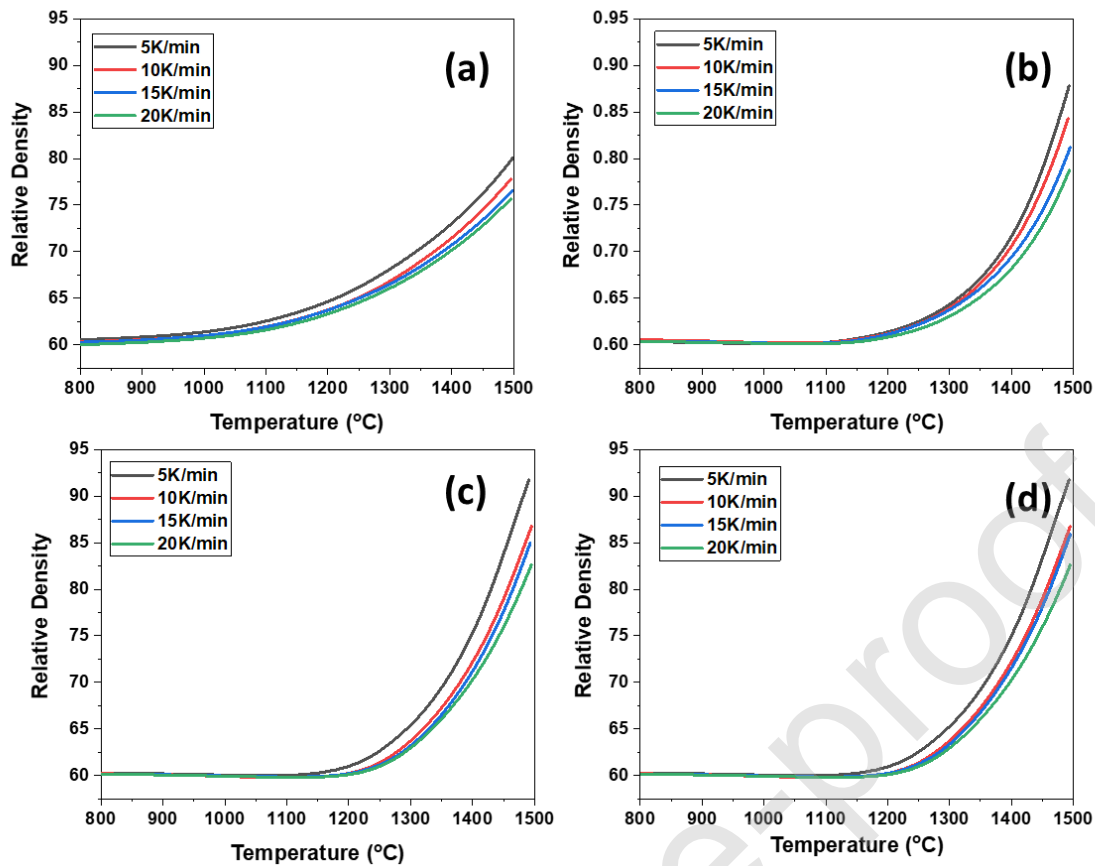


Figure 7. Variation of relative density as a function of temperature for doped and undoped samples; (a) Pure Yb_2O_3 (b) 3 mole% TiO_2 doped Yb_2O_3 (c) 5 mole% TiO_2 doped Yb_2O_3 (d) 10 mole% TiO_2 doped Yb_2O_3 .

For the different heating rates (5, 10, 15, and 20 K/min), the T and $\frac{d\rho}{dT}$ values at the same relative density were calculated and plotted as the Arrhenius-type plot of $\ln\left(T\beta\frac{d\rho}{dT}\right)$ against $1/T$. The results are shown in Fig. 8 for different values of relative densities ranging from 0.65 to 0.80. Fig. 8a is for pure Yb_2O_3 , and Fig. 8 b, c, and d for 3, 5, and 10 mole% doped samples. The activation energies for all relative densities were estimated from the slopes of these curves. From a careful look at the plots in Fig. 8, it can be seen that the lines for all relative densities (0.65-0.80) are almost parallel to each other. The results indicate that within this density range, the densification mechanism does not change. The average activation energy for pure Yb_2O_3 is 581.8 ± 47 kJ/mole. The average activation energies for TiO_2 doped samples (3, 5, and 10 mole %) are 798.9 ± 46 , 743 ± 67 , 756.7 ± 58 kJ/mole, respectively. The

large shift of activation energy for the doped sample could be due to the change in the sintering mechanism during densification. Wang and Raj also found similar trends for titania-doped alumina [23]. It can be explained either by the enthalpy of defect formation or the presence of the liquid phase at the grain boundaries. From the microstructure (Figure 2), there is no indication of the formation of liquid phase. It should also be noted that the activation energy for all levels of doping is roughly the same (within the error margin).

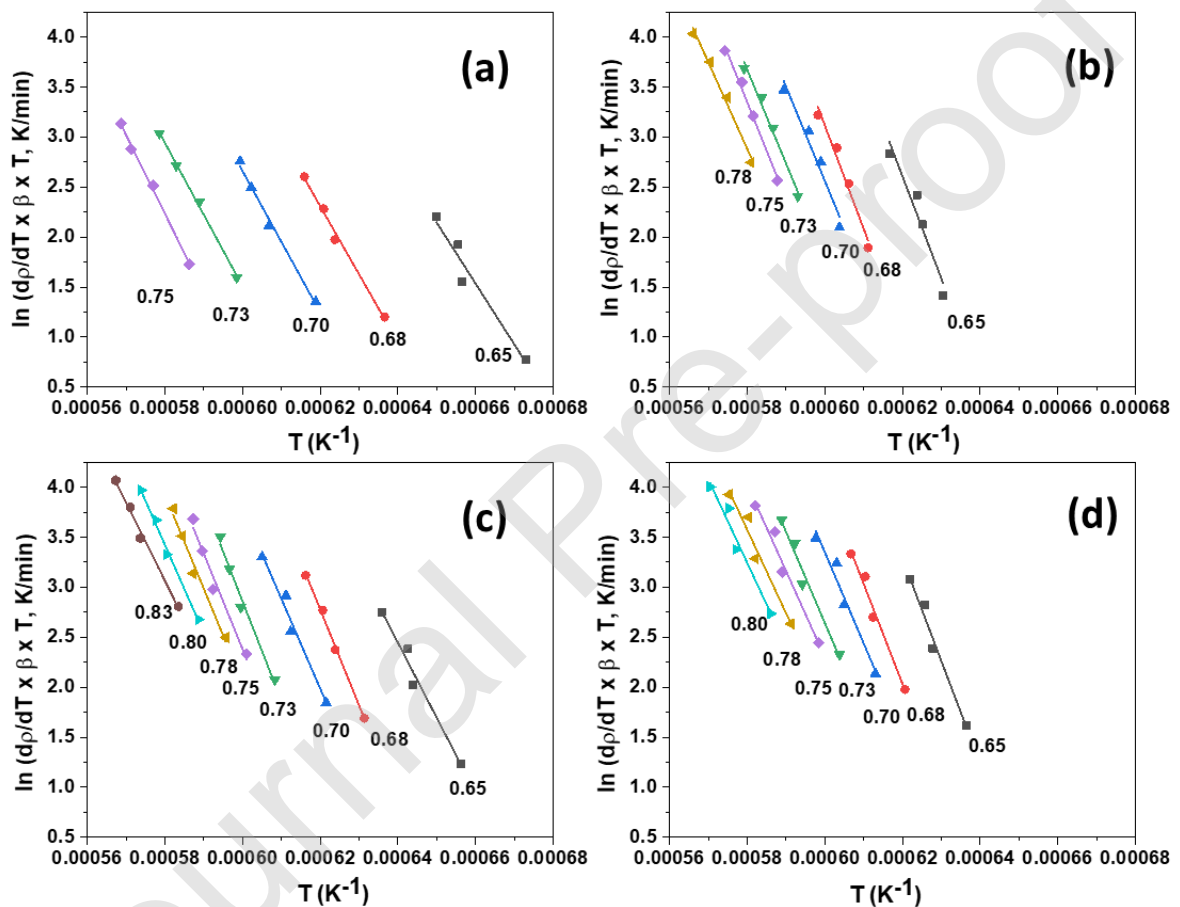


Figure 8. Arrhenius type plots of Yb_2O_3 powders with and without dopants; (a) Pure Yb_2O_3 (b) 3 mole% TiO_2 doped Yb_2O_3 (c) 5 mole% TiO_2 doped Yb_2O_3 (d) 10 mole% TiO_2 doped Yb_2O_3 .

4. Conclusions

The effect of TiO_2 doping on the densification kinetics of Yb_2O_3 was investigated. The density of sintered Yb_2O_3 increased with increasing mole percentage of TiO_2 up to 5 mole%.

The enhanced densification of was ascribed to the generation of cation vacancy and lattice distortion in the presence of Ti^{+4} ion. The solubility limit of TiO_2 in the Yb_2O_3 matrix using the results obtained from Rietveld refinement of XRD and FESEM analyses was about 5 mole %. The addition of TiO_2 up to the solid solubility limit enhances the sintering rate-controlling diffusion. Finally, using constant heating rate experiments, the activation energy for densification has been calculated, and it is shown that in the intermediate density range (60 % to 85 %), the activation energy is independent of the density. Titania doping increases the activation energy for densification.

Declaration of interests

The authors declare that they have no known competing financial interests or personal relationships that could have appeared to influence the work reported in this paper.

Acknowledgments

The authors would like to acknowledge partial support for this research from the US Department of Energy, National Energy Technology Lab (award No. DE-FE003128), and GE Gas Power. We also acknowledge insightful discussions with our colleagues from GE Gas Power Mr. John Delvaux, Mr. Matt Hafner and Mr. Joshua Margolies

References:

- [1] L. Zhao, Y.S. Hu, H. Li, Z. Wang, L. Chen, Porous $\text{Li}_4\text{Ti}_5\text{O}_{12}$ coated with N-doped carbon from ionic liquids for Li-ion batteries, *Adv. Mater.* 23 (2011) 1385–1388. doi:10.1002/adma.201003294.
- [2] Y. Zheng, Q. Lü, J. Wang, G. Zhang, Y. Gao, Z. Liu, Emission behaviors of Yb_2O_3 nanoparticles pumped by 980 nm laser at different power densities, *Opt. Laser Technol.* 63 (2014) 39–44. doi:https://doi.org/10.1016/j.optlastec.2014.03.012.
- [3] L. Longuet, A.-C. Bravo, D. Autissier, P. Vissie, J.-L. Longuet, S. Lambert, Preparation of Yb-doped Sc_2O_3 transparent ceramics for laser applications, *MRS Online Proc. Libr.* 1111 (2008) 1–6.
- [4] Y. Sohn, Yb_2O_3 nanowires, nanorods and nano-square plates, *Ceram. Int.* 44 (2018) 3341–3347. doi:https://doi.org/10.1016/j.ceramint.2017.11.118.

- [5] S. Mondal, H.-Y. Chen, J.-L. Her, F.-H. Ko, T.-M. Pan, Effect of Ti doping concentration on resistive switching behaviors of Yb_2O_3 memory cell, *Appl. Phys. Lett.* 101 (2012) 83506. doi:10.1063/1.4747695.
- [6] T.-M. Pan, C.-H. Cheng, C.-D. Lee, Yb_2O_3 Thin Films as a Sensing Membrane for pH-ISFET Application, *J. Electrochem. Soc.* 156 (2009) J108. doi:10.1149/1.3089365.
- [7] P. Kizler, H.J. Kleebe, F. Aldinger, M. Ruhle, Extended X-ray absorption fine structure (EXAFS) study of secondary phases in Yb_2O_3 -doped Si_3N_4 ceramics, *J. Mater. Sci.* 32 (1997) 369–374. doi:10.1023/A:1018501316195.
- [8] W.-H. Lee, H.-E. Kim, S.-J. Cho, Microstructural Evolution of Gas-Pressure-Sintered Si_3N_4 with Yb_2O_3 as a Sintering Aid, *J. Am. Ceram. Soc.* 80 (1997) 2737–2740. doi:10.1111/j.1151-2916.1997.tb03187.x.
- [9] N. Kondo, Y. Suzuki, T. Miyajima, T. Ohji, High-temperature mechanical properties of sinter-forged silicon nitride with ytterbia additive, *J. Eur. Ceram. Soc.* 23 (2003) 809–815. doi:https://doi.org/10.1016/S0955-2219(02)00189-9.
- [10] S. Wang, Z.H. Li, X. Liu, H. Zhang, The Effect of Yb_2O_3 Addition on Sintering of MgO Ceramic, in: *Mater. Des.*, Trans Tech Publications Ltd, 2011: pp. 1335–1338. doi:10.4028/www.scientific.net/AMR.284-286.1335.
- [11] T. Yoshioka, Y. Makino, S. Miyake, Low temperature sintering of aluminum nitride with millimeter-wave heating, *J. Mater. Sci.* 38 (2003) 101–106. doi:10.1023/A:1021118000721.
- [12] G. Magnani, F. Antolini, L. Beaulardi, E. Burrelli, A. Coglitore, C. Mingazzini, Sintering, high temperature strength and oxidation resistance of liquid-phase-pressureless-sintered SiC–AlN ceramics with addition of rare-earth oxides, *J. Eur. Ceram. Soc.* 29 (2009) 2411–2417.
- [13] W.-M. Guo, Z.-G. Yang, J. Vleugels, G.-J. Zhang, Effect of pressure loading cycle on spark plasma sintered ZrB_2 –SiC– Yb_2O_3 ceramics, *Ceram. Int.* 38 (2012) 5293–5297. doi:https://doi.org/10.1016/j.ceramint.2012.02.072.
- [14] R. Mironov, N. Georgiu, P. Kovalenko, The development of ytterbium oxide based reflective coating to reduce the heat load by thermal radiation in aircraft parts, *Mater. Today Proc.* 19 (2019) 2571–2575. doi:https://doi.org/10.1016/j.matpr.2019.08.250.
- [15] V. Manikandan, A. Vanitha, E.R. Kumar, S. Kavita, Influence of sintering temperature on structural, dielectric and magnetic properties of Li substituted CuFe_2O_4 nanoparticles, *J. Magn. Magn. Mater.* 426 (2017) 11–17.
- [16] R. Chaim, A. Shlayer, C. Estournes, Densification of nanocrystalline Y_2O_3 ceramic powder by spark plasma sintering, *J. Eur. Ceram. Soc.* 29 (2009) 91–98. doi:https://doi.org/10.1016/j.jeurceramsoc.2008.05.043.
- [17] K. Eltayeb, W. Hong, F. Chen, Y.-H. Han, Q. Shen, L. Zhang, Field-assisted sintering of multiphase toughening zirconia ceramics, *J. Ceram. Process. Res.* 18 (2017) 1–9.
- [18] W.K. Jung, H.J. Ma, D.G. Kim, D.K. Kim, Two-step sintering behavior of titanium-doped Y_2O_3 ceramics with monodispersed sub-micrometer powder, *Ceram. Int.* 45 (2019) 510–515. doi:https://doi.org/10.1016/j.ceramint.2018.09.201.
- [19] R.K. Bordia, S.-J.L. Kang, E.A. Olevsky, Current understanding and future research

- directions at the onset of the next century of sintering science and technology, *J. Am. Ceram. Soc.* 100 (2017) 2314–2352.
- [20] Y. Yang, M. Ma, F. Zhang, F. Liu, G. Chen, Z. Liu, Journal of the European Ceramic Society Low-temperature sintering of Al₂O₃ ceramics doped with 4CuO-TiO₂ - 2Nb₂O₅ composite oxide sintering aid, *J. Eur. Ceram. Soc.* 40 (2020) 5504–5510. doi:10.1016/j.jeurceramsoc.2020.06.068.
- [21] F. Zuo, S. Saunier, S. Marinell, P. Chanin-lambert, N. Peillon, D. Goeriot, Investigation of the mechanism (s) controlling microwave sintering of α -alumina : Influence of the powder parameters on the grain growth , thermodynamics and densification kinetics, *J. Eur. Ceram. Soc.* 35 (2015) 959–970. doi:10.1016/j.jeurceramsoc.2014.10.025.
- [22] A.L. Quinelato, E. Longo, L.A. Perazolli, Effect of ceria content on the sintering of ZrO₂ based ceramics synthesized from a polymeric precursor, 20 (2000) 1077–1084.
- [23] J. Wang, R. Raj, Estimate of the Activation Energies for Boundary Diffusion from Rate-Controlled Sintering of Pure Alumina, and Alumina Doped with Zirconia or Titania, *J. Am. Ceram. Soc.* 73 (1990) 1172–1175. doi:10.1111/j.1151-2916.1990.tb05175.x.
- [24] N.A. Safronova, O.S. Kryzhanovska, M. V Dobrotvorska, A.E. Balabanov, A. V Tolmachev, R.P. Yavetskiy, S. V Parkhomenko, R.Y. Brodskii, V.N. Baumer, D.Y. Kosyanov, O.O. Shichalin, E.K. Papynov, J. Li, Influence of sintering temperature on structural and optical properties of Y₂O₃–MgO composite SPS ceramics, *Ceram. Int.* 46 (2020) 6537–6543. doi:https://doi.org/10.1016/j.ceramint.2019.11.137.
- [25] L. Guo, C. Zhang, L. Xu, M. Li, Q. Wang, F. Ye, C. Dan, V. Ji, Effects of TiO₂ doping on the defect chemistry and thermo-physical properties of Yb₂O₃ stabilized ZrO₂, *J. Eur. Ceram. Soc.* 37 (2017) 4163–4169.
- [26] S. Le, S. Zhu, X. Zhu, K. Sun, Densification of Sm_{0.2}Ce_{0.8}O_{1.9} with the addition of lithium oxide as sintering aid, *J. Power Sources.* 222 (2013) 367–372. doi:https://doi.org/10.1016/j.jpowsour.2012.08.020.
- [27] J.-S. Lee, K.-H. Choi, B.-K. Ryu, B.-C. Shin, I.-S. Kim, Effects of alumina additions on sintering behavior of gadolinia-doped ceria, *Ceram. Int.* 30 (2004) 807–812. doi:https://doi.org/10.1016/j.ceramint.2003.07.018.
- [28] M. Lakusta, I. Danilenko, G. Volkova, L. Loladze, V. Burchovetskiy, T. Konstantinova, Comparative analyses of the IV group oxides additives influence on the sintering kinetics of zirconia nanopowders, *PLoS One.* 13 (2018).
- [29] M.N. Rahaman, Y.C. Zhou, Effect of solid solution additives on the sintering of ultra-fine CeO₂ powders, *J. Eur. Ceram. Soc.* 15 (1995) 939–950. doi:10.1016/0955-2219(95)00063-Z.
- [30] J.-S. Lee, K.-H. Choi, B.-K. Ryu, B.-C. Shin, I.-S. Kim, Effects of gallia additions on sintering behavior of gadolinia-doped ceria, *Mater. Res. Bull.* 39 (2004) 2025–2033. doi:https://doi.org/10.1016/j.materresbull.2004.07.022.
- [31] K. Matsui, T. Yamakawa, M. Uehara, N. Enomoto, J. Hojo, Sintering mechanism of fine zirconia powders with alumina added by powder mixing and chemical processes, *J. Mater. Sci.* 43 (2008) 2745–2753. doi:10.1007/s10853-008-2493-5.

- [32] K. Matsui, N. Ohmichi, M. Ohgai, T. Yamakawa, M. Uehara, N. Enomoto, J. Hojo, Initial Sintering Mechanism of Fine Zirconia Particles Including a Small Amount of Alumina, *J. Ceram. Soc. Japan, Suppl.* 112 (2004) S343–S349. doi:10.14852/jcersjsuppl.112.0.S343.0.
- [33] G. Suárez, Y. Sakka, Effect of alumina addition on initial sintering of cubic ZrO₂ (8YSZ), *Ceram. Int.* 36 (2010) 879–885. doi:10.1016/j.ceramint.2009.11.003.
- [34] K. Matsui, Sintering kinetics at constant rates of heating: Mechanism of silica-enhanced sintering of fine zirconia powder, *J. Am. Ceram. Soc.* 91 (2008) 2534–2539. doi:10.1111/j.1551-2916.2008.02516.x.
- [35] K. Matsui, J. Hojo, Sintering kinetics at constant rates of heating: Effect of GeO₂ addition on the initial sintering stage of 3 mol% Y₂O₃-doped zirconia powder, *J. Mater. Sci.* 43 (2008) 852–859. doi:10.1007/s10853-007-2179-4.
- [36] J. Wang, R. Raj, Activation Energy for the Sintering of Two-Phase Alumina/Zirconia Ceramics, *J. Am. Ceram. Soc.* 74 (1991) 1959–1963. doi:10.1111/j.1151-2916.1991.tb07815.x.
- [37] J. Rodriguez-Carvajal, Fullprof. 2k, Version 4.6 c--Mar 2002, *Phys. B.* 55 (1993) 192.
- [38] S.M. Salamone, L.C. Stearns, R.K. Bordia, M.P. Harmer, Effect of Rigid Inclusions on the Densification and Constitutive Parameters of Liquid-Phase-Sintered YBa₂Cu₃O_{6+x} Powder Compacts, *J. Am. Ceram. Soc.* 86 (2003) 883–892. doi:10.1111/j.1151-2916.2003.tb03392.x.
- [39] L.B. Kong, Y. Huang, W. Que, T. Zhang, S. Li, J. Zhang, Z. Dong, D. Tang, Sintering and Densification (I)---Conventional Sintering Technologies, in: *Transparent Ceram.*, Springer International Publishing, Cham, 2015: pp. 291–394. doi:10.1007/978-3-319-18956-7_5.
- [40] R.G. Bedford, E. Catalano, Investigations into the Eu-Eu₂O₃, the Eu-Pt-Eu₂O₃, the Sm-Sm₂O₃, and the Yb-Yb₂O₃ systems, *J. Solid State Chem.* 3 (1971) 112–124. doi:https://doi.org/10.1016/0022-4596(71)90014-4.
- [41] P.-L. Chen, I.-W. Chen, Grain Growth in CeO₂: Dopant Effects, Defect Mechanism, and Solute Drag, *J. Am. Ceram. Soc.* 79 (1996) 1793–1800. doi:10.1111/j.1151-2916.1996.tb07997.x.